International Journal of Mechanical, Industrial and Aerospace Sciences
ISSN: 2517-9950
Vol:10, No:8, 2016

Stabilization of a Three-Pole Active Magnetic Bearing by Hybrid Control Method in Static Mode

Mahdi Kiani, Hassan Salarieh, Aria Alasty, S. Mahdi Darbandi

***Abstract*—**The design and implementation of the hybrid control method for a three-pole active magnetic bearing (AMB) is proposed in this paper. The system is inherently nonlinear and conventional nonlinear controllers are a little complicated, while the proposed hybrid controller has a piecewise linear form, i.e. linear in each sub-region. A state-feedback hybrid controller is designed in this study, and the unmeasurable states are estimated by an observer. The gains of the hybrid controller are obtained by the Linear Quadratic Regulator (LQR) method in each sub-region. To evaluate the performance, the designed controller is implemented on an experimental setup in static mode. The experimental results show that the proposed method can efficiently stabilize the three-pole AMB system. The simplicity of design, domain of attraction, uncomplicated control law, and computational time are advantages of this method over other nonlinear control strategies in AMB systems.

***Keywords*—**Active magnetic bearing, three pole AMB, hybrid control, Lyapunov function.

I. Introduction

NOWADAYS, two parameters are important in manufacturing of rotating machinery such as machine tools, turbines and compressors, namely, speed and accuracy. In these systems, AMB is being used to achieve high rotational speeds instead of conventional bearings. AMBs have advantages such as noncontact load carrying, long life duty, no need to lubrication, ability to work in vacuum and high temperature environments, high efficiency, high speed, and so on.

The AMB system has almost a nonlinear behavior. Hence, a control technique that can stabilize the system in a large domain of attraction is the best solution for this application. Linear controllers have been extensively used by many researchers in this area. However, this type of controller can stabilize the AMB system only in a small region near the linearization point. In order to solve this problem, it is better to use a nonlinear control method. The three-pole configuration of AMB has strongly nonlinear dynamics, so a nonlinear controller is expected to have the best performance for such a system. The hybrid configuration is a conventional method to control the nonlinear systems, in which some linear controllers are matched to each other by a switching logic. In this method, the whole domain is divided into small zones, and the system is controlled by designing linear controllers for these zones. The main benefits of this method are simplicity and coverage of the total domain.

The hybrid control method has been widely used by researchers. Fierro et al. [1] used this technique to control a group of non-holonomic mobile robots with range sensors. The stability of the hybrid system that he developed is studied by using the Lyapunov theory. Karimoddini et al. [2] presented a bumpless hybrid supervisory control scheme to stabilize an unmanned helicopter. The proposed method is based on polar partitioning of the workspace. Lin-Shi et al. [3] used a hybrid control strategy to control motor drives on a permanent-magnet synchronous motor. Han et al. [4] used a hybrid feedback control to stabilize a spring-loaded inverted pendulum system. The results of this paper show that this approach has good performance on different conditions of a nonlinear system. Liu and Stechlinski [5] investigated the stabilization of a class of nonlinear systems with distributed delays using impulsive and switching control. Their criteria are based on a special type of state dependent switching law which partitions the state space into stabilizing sub-regions. A common Lyaponuv function is used to prove stability. Yuan and Wu [6] investigated the stability and L_2-gain problems for a type of linear hybrid control system by utilizing ELF[1] technique. Hybrid conditions are expressed in LMIs[2]. They used the proposed method to control an inverted pendulum example.

To control a three-pole AMB, two kinds of controller can be designed, the first one is current-control method, and the second one is voltage-control approach. Classical linear control techniques are rarely used to control and stabilize a three-pole AMB. Darbandi et al. [7] proposed linear and nonlinear output feedback controllers to stabilize a three-pole AMB system. Although the system is inherently nonlinear, Darbandi et al. showed that the system nearly has linear behavior on small displacement. Hsu and Chen [8] used the feedback linearization method to stabilize the three-pole AMB and obtained admissible domain in state space by the Lyapunov approach. Later, Chen et al. [9] presented a new current-control approach based on sliding mode method for a three-pole AMB system. The experimental results of this paper show that the rotor can be levitated to the stator axis, and its settling time is about 0.4 sec. Later, Chen and Weng [10] proposed a voltage-controlled integral sliding mode controller. In his study, the settling time is 0.5 sec, and experimental results and simulations are nearly the same.

M. Kiani is with the Department of Mechanical Engineering, Sharif University of Technology, Tehran, Iran (corresponding author, e-mail: kiani@mech.sharif.edu)

H. Salarieh, A. Alasti, and S. M. Darbandi are with the Department of Mechanical Engineering, Sharif University of Technology, Tehran, Iran (e-mail: salarieh@sharif.edu, aalasti@sharif.edu, s_m_darbandi@mech.sharif.edu)

[1] Extended Lyaponuv-like function
[2] Linear Matrix Inequalities

Chen et al. [11] implemented linear controller, feedback linearization, and integral sliding mode method on a three-pole AMB experimentally. Finally, he concluded that the linear controller is more sensitive to system parameter uncertainties and unmodeled dynamics than the sliding mode technique.

In this study, the main goal is to propose a pseudo-linear controller to stabilize a three-pole AMB system. To this end, a hybrid control method is suggested which is based on some conjunct linear controllers. The proposed technique is inherently nonlinear, but linear control methods are used to design the controller and obtain the controller gains. After that, the designed controller is implemented on a three-pole AMB experimental setup in static modes. Finally, the simulation and experimental results are presented to illustrate the performance and applicability of the proposed controller.

II. Modeling

A. Three-Pole AMB

Fig. 1 shows the schematic of the three-pole AMB that is used in this paper. The rotor is supported with a self-aligning ball bearing and the three-pole AMB. The self-aligning ball bearing allows the end of rotor to move freely in radial direction. The other end of rotor is levitated by the three-pole AMB, and the AMB is supported by a backup bearing. A flexible coupling is used to decrease the transmitted forces and moments according to misalignment. The rotor is supposed to be rigid and its dynamic can be modeled by 2-DOF rotating disk. According to the configuration of setup, the gyroscopic effect can be neglected [12].

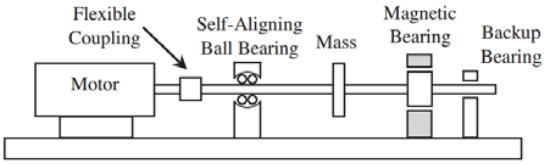

Fig. 1 Schematic of a single magnetic bearing [12]

In Fig. 2, the schematic of a three-pole AMB configuration proposed by Chen and Hsu [13] in 2002 is shown. In [14], Bouaziz et al. studied the angular misalignment and flexibility of coupling in an AMB, but in the present case, according to the above mentioned explanation, the angular misalignment between shaft and coupling and its flexibility are not considered.

The poles radially stand with an angle of 120° from each other. Each pole with the surface area A is made of copper wires and has one coil with N turns. The magnetic flux of pole j is depicted by φ_j . According to Fig. 2, the current that passes through coils 2 and 3 is the same, but this current makes opposite magnetic fluxes in their corresponding poles. When the system is in equilibrium position, the shaft axis and axis of the stator are coincident by using a bias current in the upper coils which counter-balances the weight. It should be mentioned that, in this case, two power sources are needed to produce the currents of coils and only one of them has a bias current, so this formation results in an optimum situation [7].

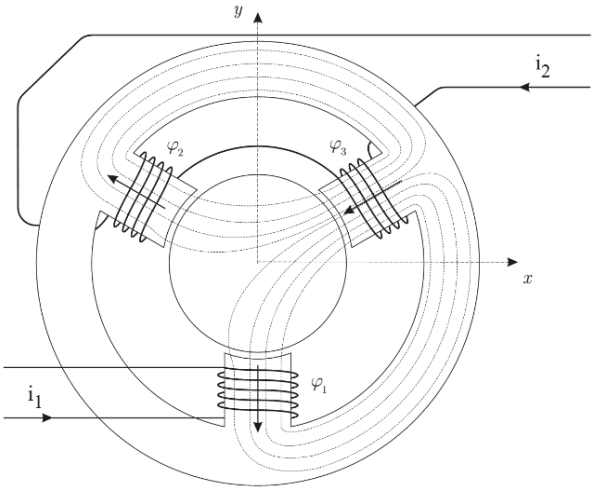

Fig. 2 Three-pole ABM with 2 coil currents [5]

Assuming no flux leakage, no saturation, and no reluctance of core (core is made of iron), the magnetic circuit diagram of the AMB is shown in Fig. 3.

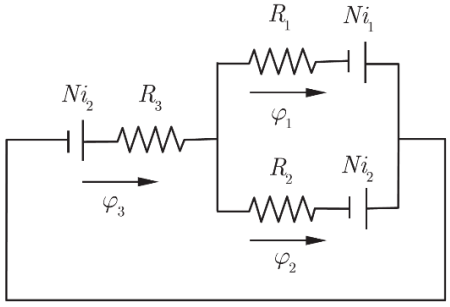

Fig. 3 Magnetic circuit of three-pole AMB [5]

With respect to Fig. 3, by using the Kirchhoff's laws, a set of equations can be derived as:

$$\begin{cases} \varphi_1 + \varphi_2 = \varphi_3 \\ Ni_2 - R_3\varphi_3 + Ni_2 - R_2\varphi_2 = 0 \\ Ni_2 - R_3\varphi_3 + Ni_1 - R_1\varphi_1 = 0 \end{cases} \quad (1)$$

where i_1 and i_2 are currents of coils, and R_j represents the reluctance, that corresponds to the air gap in each pole, which can be computed as given here:

$$R_j = \frac{s_j}{\mu_0 A} \quad , \quad j = 1,2,3 \quad (2)$$

where μ_0 is the permeability of free space whose value is $4\pi\times10^{-7}\ H.m^{-1}$, and S_j is the air gap length of each pole.

For small displacements of shaft axis, we have:

$$\begin{cases} s_1 = s_0 + y \\ s_2 = s_0 + x\sqrt{3}/2 - y/2 \\ s_3 = s_0 - x\sqrt{3}/2 - y/2 \end{cases} \quad (3)$$

where x and y are displacement of shaft axis relative to the stator, and s_0 is the nominal air gap. Substituting (3) into (2) and solving (1), three relations between coils currents, magnetic flux and displacement of shaft axis can be obtained as [7]:

$$\varphi_1 = 2\gamma\left[\sqrt{3}x i_2 + (2s_0 - y) i_1\right] \quad (4)$$

$$\varphi_2 = \gamma\left[(6s_0 - \sqrt{3}x + 3y) i_2 + (-2s_0 + \sqrt{3}x + y) i_1\right] \quad (5)$$

$$\varphi_3 = \gamma\left[(6s_0 + \sqrt{3}x + 3y) i_2 + (2s_0 + \sqrt{3}x - y) i_1\right] \quad (6)$$

$$\gamma = 2\mu_0 AN / \left(12s_0^2 - 3x^2 - 3y^2\right) \quad (7)$$

By evaluating the energy stored in the air gap and using the virtual work principal [7], [15], the magnetic force can be evaluated as:

$$f_i = \frac{\varphi_i^2}{2\mu_0 A}, \; i = 1,2,3 \quad (8)$$

In this study, the gyroscopic effect and flexibility of the supports and bases in *x* and *y* directions are ignored, so the resultant magnetic forces in *x* and *y* directions with the mentioned assumptions can be calculated as:

$$f_x = (f_3 - f_2)\sin\frac{\pi}{3} = \frac{\sqrt{3}}{4\mu_0 A}(\varphi_3^2 - \varphi_2^2) \quad (9)$$

$$f_y = (f_3 + f_2)\cos\frac{\pi}{3} - f_1 = \frac{1}{4\mu_0 A}(\varphi_3^2 + \varphi_2^2 - 2\varphi_1^2) \quad (10)$$

By substituting (4)–(7) into (9) and (10), the following equations are obtained:

$$f_x = \frac{3\gamma^2}{2\mu_0 A}\begin{bmatrix} 2x(2s_0 - y) i_1^2 + 2\sqrt{3}(x^2 - y^2 + 4s_0^2) i_1 i_2 \\ +6x(2s_0 + y) i_2^2 \end{bmatrix} \quad (11)$$

$$f_y = \frac{3\gamma^2}{2\mu_0 A}\begin{Bmatrix} \left[x^2 - (2s_0 - y)^2\right] i_1^2 + 4\sqrt{3}xy\, i_1 i_2 + \\ \left[3(2s_0 + y)^2 - 3x^2\right] i_2^2 \end{Bmatrix} \quad (12)$$

According to the above equations, it is obvious that the forces of three-pole AMB are nonlinear functions of coils current and displacements of the shaft axis that create nonlinear coupling of shaft equations in x and y directions.

The equations of the rotor in static mode can be expressed as:

$$m\ddot{x} = f_x \quad (13)$$

$$m\ddot{y} = f_y - mg \quad (14)$$

where m is the effective mass of rotor, and g is gravity acceleration.

$\bar{i}_1$ and $\bar{i}_2$ are used instead of i_1 and i_2 to counteract the weight of shaft by a bias current.

$$i_1 = \bar{i}_1 \quad (15)$$

$$i_2 = \bar{i}_2 + i_b \quad (16)$$

i_b is the bias current in the upper coils. By substituting (15) and (16) into (11) and (12), i_b can be evaluated as:

$$i_b = \frac{1}{6\gamma s_0}\sqrt{2\mu_0 Amg} \quad (17)$$

The dynamics of three coils can be described by:

$$\begin{cases} r_1 i_1 + N\dfrac{d\varphi_1}{dt} = v_1 \\ r_2 i_2 + N\left(\dfrac{d\varphi_1}{dt} + \dfrac{d\varphi_2}{dt}\right) = v_2 \end{cases} \quad (18)$$

where r_1 is resistance of coil 1 (bottom coil), and r_2 is the resistance of coils 2 and 3 (upper coils). Equations (13), (14), and (18) model the equations of the three-pole AMB.

III. Hybrid Control

A. Controller Design

To design the controller by the hybrid method, the system equations should be expressed in PWA[3] form. In PWA formulation, the working area is divided into some sub-regions, then in each sub-region, the nonlinear system is linearized about a point in the corresponding sub area [16], [17]. In this paper, the total region is divided into 13 sub-regions with linearization point on each region, and when the number of sub-regions increases, the performance of system improves [18]. In each region the controller is designed by using the LQR method, and after that, the system is simulated.

[3] Piecewise Affine

$$\dot{X} = A_i (X - X_0) + B_i (u - u_0) + f(X_{0_i}, u_0) + hot_i \quad ,$$
$$E_i X + D_i < 0 \quad i = 1,...,13 \tag{19}$$
$$Y = [x \quad y]^T$$
$$A_i = \frac{\partial f}{\partial X}(X_{0_i}, u_{0_i}) \quad , \quad B_i = \frac{\partial f}{\partial u}(X_{0_i}, u_{0_i}) \quad , \quad i = 1,...,13 \tag{20}$$

The matrices A_i and B_i are derived from the linearization of nonlinear equations, X_{0_i} is the linearization point that is shown in Fig. 4, and hot_i depicts high order terms of nonlinear equation after linearization. For all of sub-regions, $u_{0_i} = [0 \quad 0]^T \quad i = 1,...,13$. $E_i X + D_i < 0$ defines each sub-region; in the other words, this inequality specifies switching of controller. $E_i X + D_i = 0$ depicts the switching boundary.

To explain the system in state space, the state variables are chosen as:

$$x_1 = i_1 \ , \ x_2 = i_2 \ , \ x_3 = x$$
$$x_4 = \dot{x} \ , \ x_5 = y \ , \ x_6 = \dot{y} \tag{21}$$

In the linearization points, states of x_1, x_4, x_6 are equal to zero, x_2 is i_b, and x_3, x_5 are shown in Fig. 4. In this figure, the sub-regions, switching boundaries, and the linearization points of sub-regions are shown. These sub-regions are obtained by try and error in this paper. The configuration of sub-regions impresses the controller performance. Researchers can study about configuration of zones to optimize the performance. In fact, the work space of the shaft is limited by backup bearing into a circle with 0.5 mm radius.

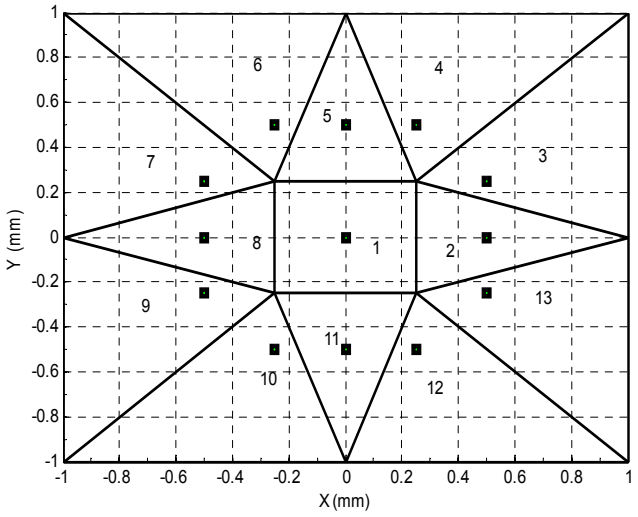

Fig. 4 The zoning and linearization points in x-y plane

In this study, the controller and observer are designed, and their combination is used. In the other words, to get feedback in the controller, the states of observer are used. To control this system a linear feedback controller is designed as:

$$u_i = -K_i \begin{bmatrix} \hat{X} \\ x_7 \\ x_8 \end{bmatrix} + m_i \qquad i = 1,...,13 \tag{22}$$

where K_i is controller gain, m_i is constant for the controller in each region, and m_i sets the equilibrium point of each sub-system defined by (19) and (22) to the origin, because the system should not be stabilized in the current sub-region. State variables x_7 and x_8 are the integrator terms in the following form:

$$x_7 = \int x_3 dt$$
$$x_8 = \int x_5 dt \tag{23}$$

After adding the above states to X, new vector $\bar{X}^T = [X^T \quad x_7 \quad x_8]$ is defined, and according to this definition, other system matrices are obtained as:

$$\bar{A}_i = \begin{bmatrix} A_i & 0_{2\times 6} \\ \bar{I}_{6\times 2} & 0_{2\times 2} \end{bmatrix}, \ \bar{I}_{6\times 2} = [0_{2\times 2} \quad I_{2\times 2} \quad 0_{2\times 2}] \tag{24}$$
$$\bar{B}_i = [B_i \quad 0 \quad 0]^T \tag{25}$$

where $I_{2\times 2}$ is an identity matrix.

Feedback gains are obtained by using LQR method. To this end, the following cost function is considered:

$$J = \int_0^\infty \left(\bar{X}^T Q \bar{X} + u^T R u \right) dt \tag{26}$$

in which R and Q are positive definite weight matrices. The optimal gain of controller for each sub-region when the performance index is given by (26) is obtained as [19]:

$$K_i = R^{-1} \bar{B}_i^T P_i \tag{27}$$

where P_i is the unique positive definite solution of the steady state Riccati equation:

$$\bar{A}_i^T P_i + P_i \bar{A}_i - P_i \bar{B}_i R^{-1} \bar{B}_i^T P_i + Q = 0 \tag{28}$$

To make trajectories converge to the main equilibrium point that is in sub-region 1, the equilibrium point of each sub-system (19) and (22) has not to be in its corresponding domain, and these points must be coincident on the origin. Now, for this purpose, constant terms of controllers, m_i, are selected as:

$$m_i = \left(B_i{}^T B_i \right)^{-1} B_i \begin{pmatrix} A_i X_{0_i} + B_i u_{0_i} - \\ f\left(X_{0_i}, u_{0_i}\right) - A_i X_{0_1} \end{pmatrix} \tag{29}$$

B. Observer Design

The position of shaft end that is levitated by three-pole AMB and the coil currents are measurable states. Shaft position is measured with proximity sensors, and coil currents are obtained by using the Hall sensors. The coil currents signal are very noisy and cannot be used in feedback control law [7]. The proximity sensors measurements are quite noisy, Sun et al. in [20] proposed a soft sensing method based on support vector regression and Extended Kalman filter that can estimate the displacement precisely. In this study, the proximity sensors data are used in control law directly. Moreover, measuring the velocity of shaft is not possible, therefore, for the mentioned reasons, an observer has to be used for estimating the states of system. The equations of observers are given by:

$$\dot{\hat{X}} = A_i \hat{X} + B_i \bar{u} + K_{o_i} \left(Y - \hat{Y} \right), \; E_i X + D_i < 0 \quad i = 1,...,1 \tag{30}$$

$$\hat{Y} = C\hat{X} \quad , \quad C = \begin{bmatrix} 0 & 0 & 1 & 0 & 0 & 0 \\ 0 & 0 & 0 & 0 & 1 & 0 \end{bmatrix} \tag{31}$$

where A_i , B_i and C are linearized system matrices, K_{o_i} is the observer gain in each sub-region, and $\bar{u} = -\hat{K}_i \hat{X}$. $\hat{K}_i$ has the following form:

$$\hat{K}_i = \begin{bmatrix} K_{i_{11}} & K_{i_{12}} & K_{i_{13}} & K_{i_{14}} & K_{i_{15}} & K_{i_{16}} \\ K_{i_{21}} & K_{i_{22}} & K_{i_{23}} & K_{i_{24}} & K_{i_{25}} & K_{i_{26}} \end{bmatrix} \tag{32}$$

in which $K_{i_{mn}}$ is the element of $\hat{K}_i$. The three-pole AMB system is observable in each sub-region. In the other words, the observability matrix is full rank for this system in each sub-region. The observability matrix for each linearized zone is as:

$$N_i = \begin{bmatrix} C \\ CA_i \\ CA_i{}^2 \\ CA_i{}^3 \\ CA_i{}^4 \\ CA_i{}^5 \end{bmatrix} \tag{33}$$

The observer gains are calculated by pole placement method. The poles are set four times or five times greater than the poles of controllers to have a suitable performance.

The estimation error is the difference between the system states and observer states, therefore the error dynamics can be written as:

$$e = X - \hat{X} \tag{34}$$

$$\dot{e} = \left(A_i - K_{o_i} C \right) e + hot_i \tag{35}$$

If the estimation error converges to zero, the observer estimates the system states. The stability proof of the observer/controller system is expressed in the next section.

IV. Result

A. Simulation Results

The simulation results for the three-pole AMB are presented in this section. The model that is given by (13), (14) and (18) is used to simulation. The nominal parameters of the system are expressed in Table I, which are also the parameters of the experimental setup.

The matrices utilized in the LQR cost function are selected by a trial and error process as:

$$Q = \begin{bmatrix} Q_1 & 0 \\ 0 & Q_2 \end{bmatrix}, \; R = \begin{bmatrix} 2 & 0 \\ 0 & 0.1 \end{bmatrix} \tag{36}$$

where Q_1 and Q_2 are diagonal matrices and they are given as:

$$\begin{aligned} Q_1 &= diag\left[1,1,5,1\right] \\ Q_2 &= diag\left[5\times10^4, 1, 5\times10^8, 10^7\right] \end{aligned} \tag{37}$$

TABLE I
PARAMETERS OF THE EXPERIMENTAL SYSTEM

Symbol	Description	Value
s_0	Nominal air gap	1.0 mm
N	Coil turns	350
A	Pole face area	4.5×10^{-4} m^2
d_s	Shaft diameter	30 mm
l	Shaft length	550 mm
d_r	Magnetic bearing rotor diameter	70 mm
s_b	Backup bearing (Supporting bearing) nominal air gap	0.5 mm
m	Effective mass of the shaft	1.4kg
me	Product of mass and Eccentricity of mass center	100×10^{-6} kg.m

The results are shown in static mode. The initial conditions for state variables for simulation are:

$$\begin{aligned} &i_{l_0}=0 \quad i_{2_0}=0 \\ &x=0.1\ mm \quad \dot{x}=0 \\ &y=-0.5\ mm \quad \dot{y}=0 \end{aligned} \tag{38}$$

and the initial conditions for the observer are:

$$\begin{aligned} &\hat{i}_{l_0}=0 \quad \hat{i}_{2_0}=0 \\ &\hat{x}=0 \quad \dot{\hat{x}}=0 \\ &\hat{y}=0 \quad \dot{\hat{y}}=0 \end{aligned} \tag{39}$$

1. Hybrid Technique

The results of system simulation with hybrid controller based on the above equations and initial conditions are given in the following figures. Fig. 5 shows the steady state of system trajectory for shaft.

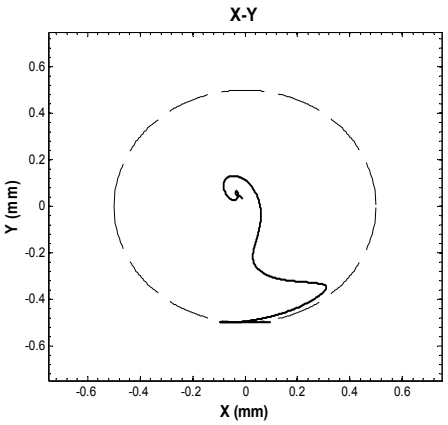

Fig. 5 Shaft trajectory obtained by implementing hybrid control in dynamic mode

In simulation, it has been tried that the real conditions which govern the experimental test are considered. According to these conditions, the results of simulating system are presented in Fig. 6. According to TABLE I, the nominal air gap is 1 mm, and the shaft does not collide with the supporting bearing.

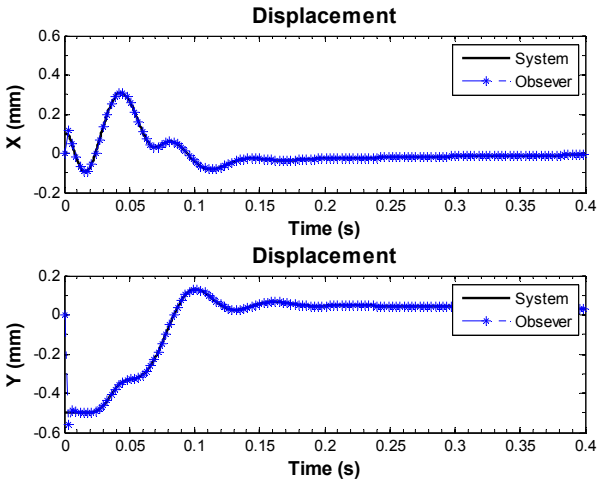

Fig. 6 Displacement of shaft in X and Y directions and their estimating by implementing hybrid control in dynamic mode

To control the system in this situation, a control command is needed, and this input is depicted in Fig. 7. The required control signals to stabilize the system are two voltages applied to the power-supply of the three-pole AMB coils.

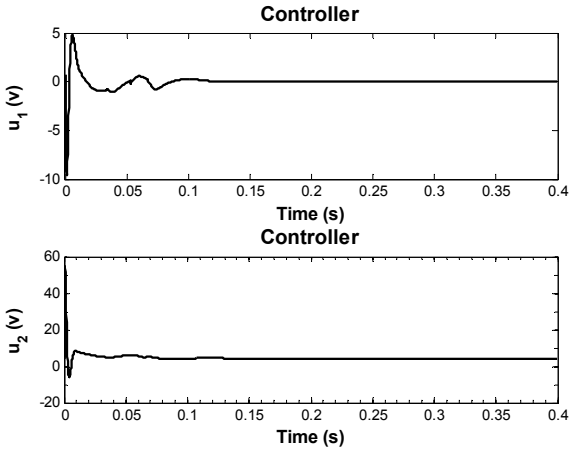

Fig. 7 Analog voltage of power amplifier for hybrid controller in dynamic mode

Fig. 8 shows the power consumption versus time in hybrid control.

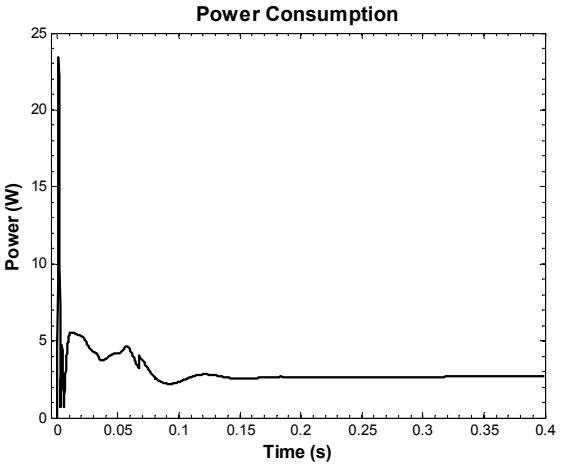

Fig. 8 Power consumption of coils for hybrid controller in dynamic mode

2. Non-Hybrid Linear Technique

If the nonlinear system is linearized around the equilibrium point of three-pole AMB system, the linearized matrices of sub-region 1 is obtained. Now, if the proposed matrices of the LQR method are used to design a simple non-hybrid linear controller for the system, the simulation results are obtained like the ones presented in the following figures. For the initial conditions that are introduced above, Fig. 9 shows the behavior of system in $X-Y$ coordinates. In this figure, the collision with backup bearing is seen at the beginning of stabilization.

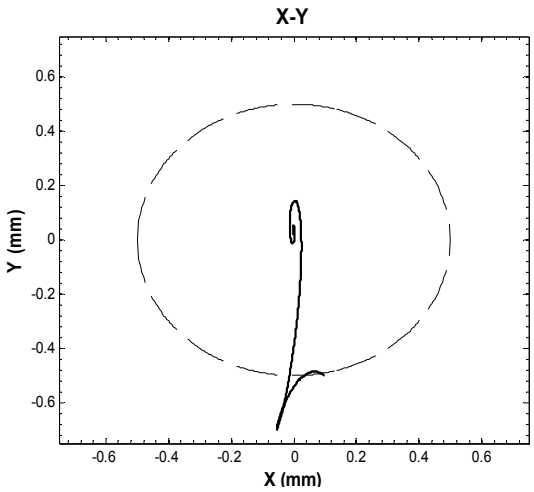

Fig. 9 Shaft trajectory obtained by implementing a simple non-hybrid linear control in dynamic mode

The results of simulation in X and Y directions are indicated in Fig. 10. This figure shows that the observer can estimate the state of x and y.

The power consumption of three coils are obtained for the simple linear controller. This result is shown in Fig. 12.

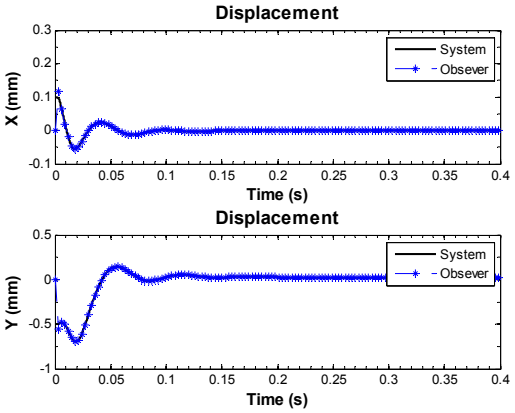

Fig. 10 Displacements of shaft in X and Y directions and their estimating by implementing the simple non-hybrid linear control in dynamic mode

The input voltages are presented in Fig. 11. The behavior of controllers can be seen versus time.

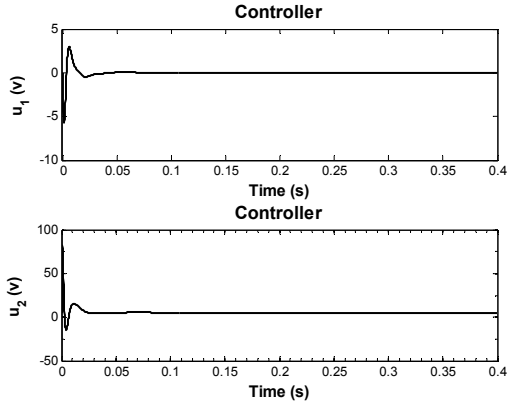

Fig. 11 Analog voltage of power amplifier for the simple non-hybrid linear controller in dynamic mode

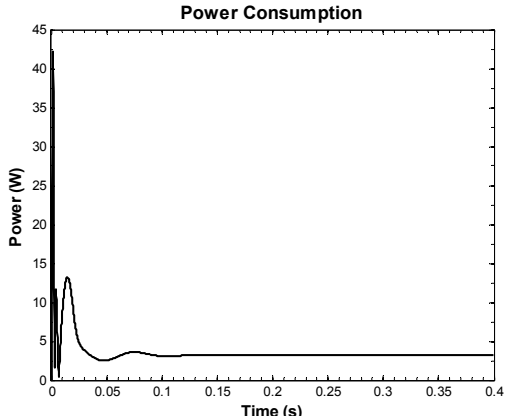

Fig. 12 Power consumption of coils for linear controller in dynamic mode

According to above results for non-hybrid linear and hybrid controller, the voltage usage can be decreased in the hybrid

technique compared to the linear method. Moreover, power used to control the three-pole AMB is decreased by using hybrid technique and by increasing number of sub-regions. Integrating the power consumption yields the total used energy for 0 to 0.4 sec. The energy consumption in hybrid method is $1.2014\,J$, and the used energy of linear control is $1.4718\,J$.

B. Experimental Results

To check the effectiveness of the hybrid method, hybrid controller is applied to a three-pole AMB system. To compare the hybrid method with the simple non-hybrid linear technique, the linear controller is implemented on the setup. Figs. 14 and 13 show the experimental setup of three-pole AMB.

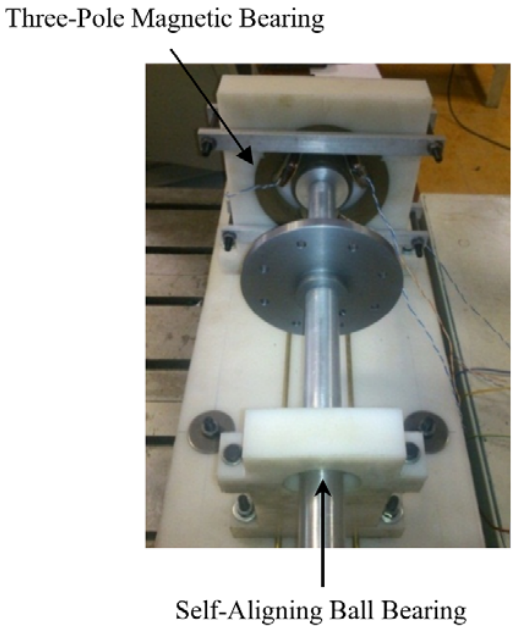

Fig. 13 Three-pole AMB [5]

The hybrid controller designed in the previous section is applied to the real system. The system has two proximity sensors for measuring the position of rotor axis and two Hall-effect sensors to measure the coils current. In the proposed controller, the displacement values measured by proximity sensors are used to switch controller. The hybrid controller is tested on the experimental setup for static mode. The proximity sensors can sense subject in 0.5 mm until 2.5 mm and give the output signal in the range of 0-10 V. In the other words, 0.5 mm to 2.5 mm is the working area of sensor, and the displacement of any object in this area is measured by sensors. To this end, the sensors are mounted in adequate distance from the rotor. The sensors used in this experiment setup are Balluff model: BAW M08EI-UAD25F-BP03 has the accuracy of $10\,\mu m$. The Hall-effect sensors have 80 kHz bandwidth and they are sensitive to 66-185 mV/A output. The discretization time in this study is 150 microseconds.

The controller has been designed in continuous space but the controller devices and sensors work digitally. Then, the hybrid controller is implemented in digital technique on experimental setup. In the digital control, the controlling bandwidth is limited by accuracy of devices and sensors.

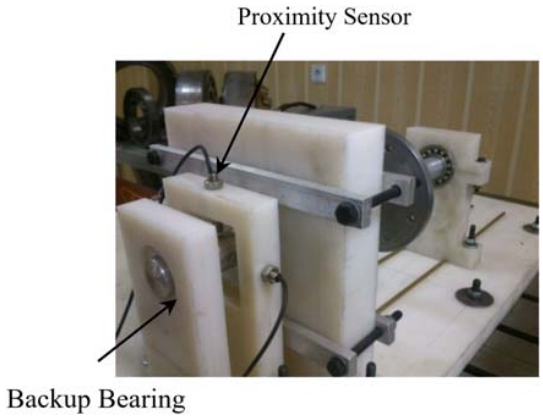

Fig. 14 Experimental setup of three-pole AMB [5]

To measure the shaft position, inductive proximity sensors are used in x and y directions as depicted in Fig. 14. The digital controller consists of a 12 bit A/D, a D/A convertor, and a PC with a Pentium IV processor running at 2.8 GHz under RTAI, a real-time open source application interface operating system that works on Linux. To apply the designed controller on the experimental model in real-time control for the AMB with a frequency of 5 kHz, the C++ programming language and RTAI extension of Linux operating system are used.

The coils are driven by two PWM power amplifiers with the switching frequency of 22 kHz. These power amplifiers provide maximum continuous output current of 10 A. The power supply delivers 24 V for proximity sensors and 40 V for the power amplifier.

As mentioned earlier, the gyroscopic effect and flexibility of supports and bases are not considered in modeling of the proposed three-pole AMB. The designed controller can stabilize the system and it shows that the presented approach is efficient and applicable.

3. Hybrid Technique

Fig. 15 shows the trajectory of system in the absence of rotation. Here, the controller can bring the rotor axis to the stator axis. After activating the controller, the current in upper coils is increased to produce the required force for overcoming the shaft weight. When the current of the upper coils reaches to its bias value, the shaft starts to move toward the bearing axis. Fig. 15 shows that the proposed controller can stabilize the three-pole AMB system.

Horizontal and vertical displacements of the shaft versus time are shown in Fig. 16. From this figure, it can be concluded that the observer can estimate well the state variables of the real system using the data obtained from the sensors measurements.

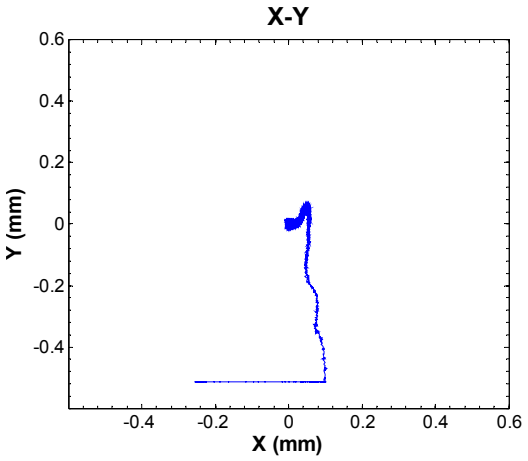

Fig. 15 Trajectory of shaft axis in experimental test for the hybrid method in the static mode

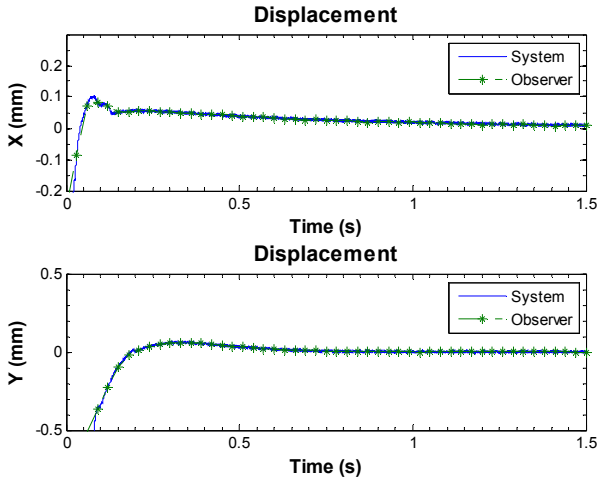

Fig. 16 Trajectory of shaft axis in experimental test for the hybrid method in the static mode

The input voltages of the hybrid-linear feedback controller are illustrated in Fig. 15. One of the most important features of a controller is its magnitude required to stabilize the system. In magnetic bearings, it is very important that the coils current does not increase beyond the saturation limit of the magnetic core.

Each coil requires power to supply voltage and current for it. The power consumption of two coils is shown in Fig. 18 for the hybrid controller. The total energy that is used in 10 seconds to control the system in hybrid technique equals $6.7493\,J$.

4. Non-Hybrid Linear Technique

To compare the simple non-hybrid linear control with the hybrid control, the obtained linear controller in the previous sections, is applied on the experimental setup. Fig. 19 shows the trajectory of system for the static mode. In this figure, it can be seen that the shaft axis is led to the equilibrium position.

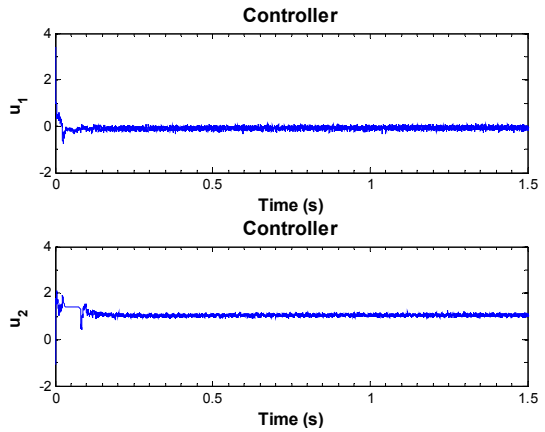

Fig. 17 Control signal in experimental test that control the system for the hybrid method in the static mode

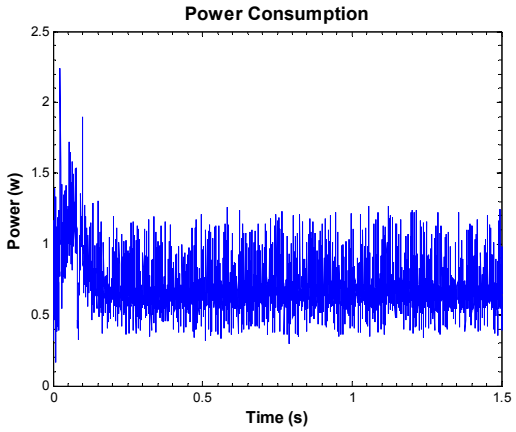

Fig. 18 Power consumption for hybrid method in the static mode

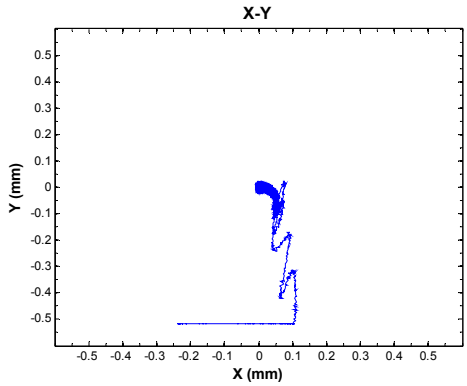

Fig. 19 Trajectory of shaft axis in experimental test for the linear method in the static mode

The horizontal and vertical displacements of the shaft versus time are shown in Fig. 20. From this figure, it can be said that the observer can predict well the state variables of the real system using the data obtained from the sensors measurements.

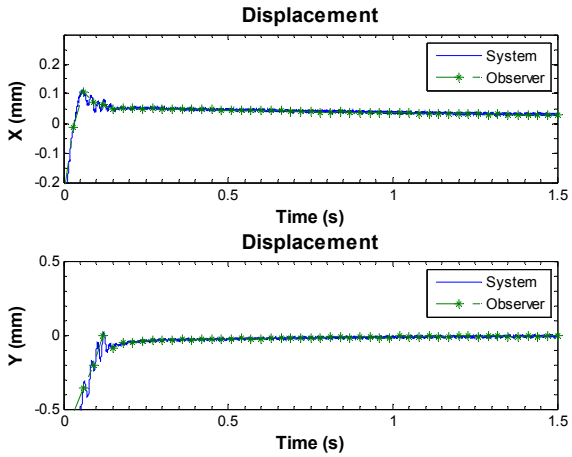

Fig. 20 Trajectory of shaft axis in experimental test for the non-hybrid linear method in the static mode

The input voltages of the linear controller are illustrated in Fig. 21. The maximum input voltage on non-hybrid linear method is $3.5V$, and the maximum voltage of hybrid controller is $2V$.

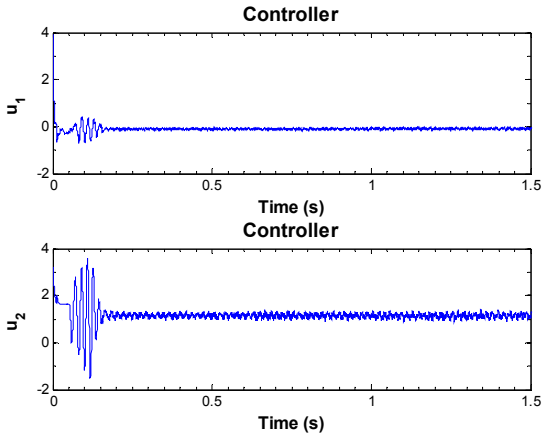

Fig. 21 Control signal in experimental test that control the system for the non-hybrid linear method in the static mode

Each coil requires power to supply voltage and current for it. The power consumption of two coils is shown in Fig. 22 for the no-hybrid linear method. The total energy that is used in 10 seconds to control the system in this technique equals $8.1188J$. The consumed energy has been increased in non-hybrid linear method comparing to the hybrid technique.

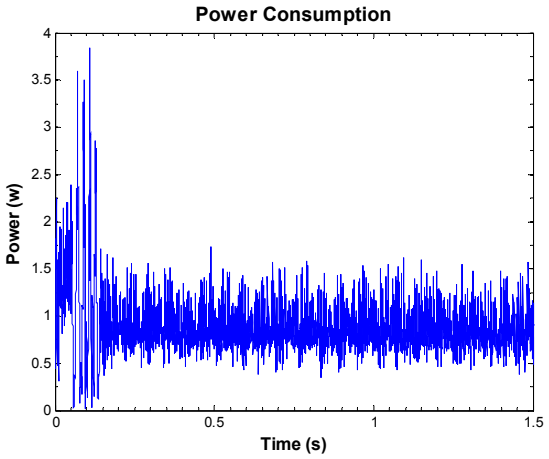

Fig. 22 Power consumption for the non-hybrid linear method in the static mode

V. Conclusion

Design and implementation of hybrid controller for an experimental three-pole AMB model have been presented in this study. It is shown that a linear hybrid control method can be used and applied to three-pole AMB as a nonlinear controller method. The gains of controller are set by LQR method for each sub-region and the observer gains are derived by the pole placement method. Darbandi in [7], compare the linear controller with integral sliding mode and concluded that the linear controller has better performance and short computational time against integral sliding mode method. For this purpose, a non-hybrid linear controller is designed by LQR technique and then implemented on AMB setup to compare it with hybrid control. According to experimental results, hybrid control method uses less voltage and power to stabilize the rotor compared to non-hybrid linear technique. Simulation and experimental results show the effectiveness of the proposed method. An important advantage of this method compared to other nonlinear methods is its simplicity in design and application.

References

[1] R. Fierro, A. K. Das, V. Kumar, and J. P. Ostrowski, "Hybrid control of formations of robots," in *Robotics and Automation, 2001. Proceedings 2001 ICRA. IEEE International Conference on*, 2001, pp. 157-162.

[2] A. Karimoddini, H. Lin, B. M. Chen, and T. H. Lee, "A bumpless hybrid supervisory control algorithm for the formation of unmanned helicopters," *Mechatronics,* vol. 23, pp. 677-688, 9// 2013.

[3] X. Lin-Shi, F. Morel, A. M. Llor, B. Allard, and J.-M. Retif, "Implementation of hybrid control for motor drives," *Industrial Electronics, IEEE Transactions on,* vol. 54, pp. 1946-1952, 2007.

[4] B. Han, X. Luo, Q. Liu, B. Zhou, and X. Chen, "Hybrid control for SLIP-based robots running on unknown rough terrain," *Robotica,* vol. 32, pp. 1065-1080, 2014.

[5] X. Liu and P. Stechlinski, "Hybrid control of impulsive systems with distributed delays," *Nonlinear Analysis: Hybrid Systems,* vol. 11, pp. 57-70, 1// 2014.

[6] C. Yuan and F. Wu, "Analysis and synthesis of linear hybrid systems with state-triggered jumps," *Nonlinear Analysis: Hybrid Systems,* vol. 14, pp. 47-60, 11// 2014.

[7] S. M. Darbandi, M. Behzad, H. Salarieh, and H. Mehdigholi, "Linear Output Feedback Control of a Three-Pole Magnetic Bearing," pp. 1323-1330, 2013.
[8] C.-T. Hsu and S.-L. Chen, "Exact linearization of a voltage-controlled 3-pole active magnetic bearing system," *Control Systems Technology, IEEE Transactions on,* vol. 10, pp. 618-625, 2002.
[9] S.-L. Chen, S.-H. Chen, and S.-T. Yan, "Stabilization of a current-controlled three-pole magnetic rotor-bearing system by integral sliding mode control," in *Networking, Sensing and Control, 2004 IEEE International Conference on*, 2004, pp. 949-954.
[10] S.-L. Chen and C.-C. Weng, "Robust control of a voltage-controlled three-pole active magnetic bearing system," *Mechatronics, IEEE/ASME Transactions on,* vol. 15, pp. 381-388, 2010.
[11] S.-L. Chen, S.-H. Chen, and S.-T. Yan, "Experimental validation of a current-controlled three-pole magnetic rotor-bearing system," *Magnetics, IEEE Transactions on,* vol. 41, pp. 99-112, 2005.
[12] S. M. Darbandi, M. Behzad, H. Salarieh, and H. Mehdigholi, "Harmonic disturbance attenuation in a three-pole active magnetic bearing test rig using a modified notch filter," *Journal of Vibration and Control,* p. 1077546315586494, 2015.
[13] S.-L. Chen and C.-T. Hsu, "Optimal design of a three-pole active magnetic bearing," *Magnetics, IEEE Transactions on,* vol. 38, pp. 3458-3466, 2002.
[14] S. Bouaziz, N. Belhadj Messaoud, J.-Y. Choley, M. Maatar, and M. Haddar, "Transient response of a rotor-AMBs system connected by a flexible mechanical coupling," *Mechatronics,* vol. 23, pp. 573-580, 9// 2013.
[15] G. Schweitzer, H. Bleuler, E. H. Maslen, M. Cole, P. Keogh, R. Larsonneur*, et al.*, *Magnetic bearings: theory, design, and application to rotating machinery*: Springer, 2009.
[16] L. Rodrigues and S. Boyd, "Piecewise-affine state feedback for piecewise-affine slab systems using convex optimization," *Systems & Control Letters,* vol. 54, pp. 835-853, 2005.
[17] L. Rodrigues and J. P. How, "Observer-based control of piecewise-affine systems," *International Journal of Control,* vol. 76, pp. 459-477, 2003.
[18] A. Hassibi, J. How, and S. Boyd, "A path-following method for solving BMI problems in control," in *American Control Conference, 1999. Proceedings of the 1999*, 1999, pp. 1385-1389.
[19] D. E. Kirk, *Optimal control theory: an introduction*: Courier Corporation, 2012.
[20] Z. Sun, J. Zhao, Z. Shi, and S. Yu, "Soft sensing of magnetic bearing system based on support vector regression and extended Kalman filter," *Mechatronics,* vol. 24, pp. 186-197, 4// 2014.